Modulating the electro-optical properties of doped C_3N monolayers and graphene bilayersviamechanical strain and pressure

Reference:
Bafekry Asadollah, Nguyen C., Obeid M. M., Ghergherehchi M..- Modulating the electro-optical properties of doped C_3N monolayers and graphene bilayersviamechanical strain and pressure
New journal of chemistry - ISSN 1144-0546 - 44:36(2020), p. 15785-15792
Full text (Publisher's DOI): https://doi.org/10.1039/D0NJ03340E
To cite this reference: https://hdl.handle.net/10067/1719360151162165141

NJC

New Journal of Chemistry

A journal for new directions in chemistry

Accepted Manuscript

This article can be cited before page numbers have been issued, to do this please use: A. Bafekry, C. Nguyen, M. Obeid and M. Ghergherehchi, *New J. Chem.*, 2020, DOI: 10.1039/D0NJ03340E.

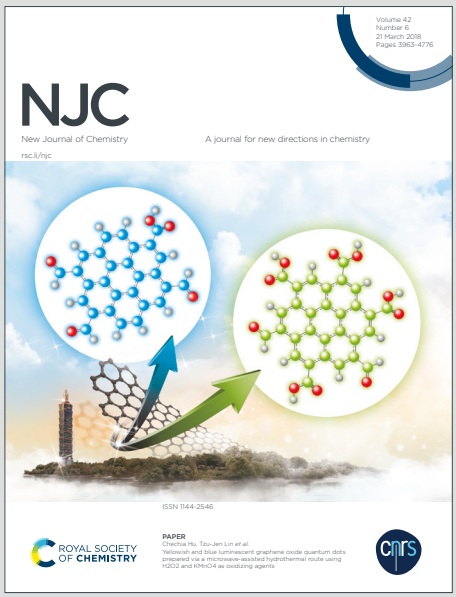

This is an Accepted Manuscript, which has been through the Royal Society of Chemistry peer review process and has been accepted for publication.

Accepted Manuscripts are published online shortly after acceptance, before technical editing, formatting and proof reading. Using this free service, authors can make their results available to the community, in citable form, before we publish the edited article. We will replace this Accepted Manuscript with the edited and formatted Advance Article as soon as it is available.

You can find more information about Accepted Manuscripts in the Information for Authors.

Please note that technical editing may introduce minor changes to the text and/or graphics, which may alter content. The journal's standard Terms & Conditions and the Ethical guidelines still apply. In no event shall the Royal Society of Chemistry be held responsible for any errors or omissions in this Accepted Manuscript or any consequences arising from the use of any information it contains.

View Article Online
DOI: 10.1039/D0NJ03340E

Journal Name

ARTICLE TYPE

Cite this: DOI: 10.1039/xxxxxxxxxx

Modulating the electro-optical properties of doped C_3N monolayer and graphene bilayer via mechanical strain and pressure

A. Bafekry[1,2†], C. Nguyen[3], M. M. Obeid[4], M. Ghergherehchi[5†]

Received Date
Accepted Date

DOI: 10.1039/xxxxxxxxxx

www.rsc.org/journalname

In this work, we investigated systematically the electronic and optical properties of B doped C_3N monolayer as well as B and N doped graphene bilayer ($BN-Gr@2L$). We found that the doping of B atom leads to an enlarged band gap of C_3N monolayer and when the dopant concentration reaches to 12.5%, a indirect-to-direct band gap switching is occurred. In addition, with co-doping of B and N atoms on graphene monolayer in the hexagonal configuration, an electronic transition from semi-metal to semiconductor is occurred. Our optical results for the B-C_3N shows a broad absorption spectrum in a wide visible range start from 400 nm to 1000 nm with strong absorption intensity, making it suitable candidate for nanoelectronic and optoelectronic applications. Interestingly, a transition from semi-metal to semiconductor is emerged in the graphene monolayer with doping of B and N atoms. Furthermore, our results demonstrate that in-plane strain and out-of-plane strain (pressure) can modulate the band gap of the $BN-Gr@2L$. The controllable electronic properties as band gap and optical features of the doped graphene bilayer by strain engineering may facilitate their practical performance for future various applications.

1 Introduction

Following the development of materials science, a lot of new materials with appropriated physical and chemical properties that are required for the design of high-performance nanodevices have been predicted and synthesized. The discovery of graphene[1] in 2004 by Geim and his group has opened up a new chapter for thin film two-dimensional materials (2DM), which can be considered as promising candidate for various applications, including optoelectronic, photocatalyst, gas sensors, light-emitting diodes[2–5]. To now, there are many 2DM, including hexagonal boron nitride (hBN)[6,7], phosphorene[8,9], transition metal dichalcogenides (TMDCs)[10–13] and graphitic carbon nitrides[14,15]. However, the most of 2DM in their freestanding monolayers have a drawback that may hinder their applications in high-efficient devices. For instance, the lack of an electronic band gap in graphene makes it incompatible with high-speed logic circuit devices[16]. Molybdenum disulfide (MoS_2) is one of the most famous TMDCs, it exhibits a semiconducting nature with a suitable band gap of about 2 eV for semiconductor energy devices[17]. Unfortunately, due to a small carrier mobility of about 200 cm^2/Vs, MoS_2 monolayer is incompatible with high-performance nanoelectronic devices[18]. Therefore, along with the design and synthesis of new 2DM, one of the most important tasks for research on 2DM is how to tune the properties and extend the range of applications of these 2DM.

Recently, element doping has been proved to be one of the most strategies to modify the physicochemical properties of graphene and the formation of novel graphene-like 2DM. Porous graphitic carbon nitrides, such as C_2N, C_3N_4, and C_3N monolayers have attracted considerable interest because of their intriguing physical and chemical characteristics, including on/off current ratio[19], high thermal conductivity[20]. For instance, a high on/off ratio of 10^7 of C_2N monolayer makes its suitable for the design of the field-effect transistor[19]. Wang et al.[21] demonstrated that C_3N_4 monolayer can be considered as a photocatalyst for hydrogen production. More recently, a newly fabricated 2D C_3N material has been synthesized experimentally[22,23] by a hydrothermal treatment. An indirect band gap of 0.39 eV and a high on/off ratio of 5.5×10^10 make the C_3N monolayer promising candidate for field-effect transistor[23].

[1]Department of Physics, University of Guilan, 41335-1914 Rasht, Ira. E-mail: bafekry.asad@gmail.com
[2]Department of Physics, University of Antwerp, Groenenborgerlaan 171, B-2020 Antwerp, Belgium
[3]Institute of Research and Development, Duy Tan University, Da Nang 550000, Vietnam.
[4]Department of Ceramics, College of Materials Engineering, University of Babylon, 51002, Hilla, Iraq
[5]College of Electronic and Electrical Engineering, Sungkyun kwan University, Suwon, Korea. Email: mitragh@skku.edu
† To whom correspondence should be addressed.

View Article Online
DOI: 10.1039/D0NJ03340E

The electronic, magnetic and magnetic characteristics of 2D C_3N monolayer are very sensitive to strain[24], doping[25], functionalization[26], and stacking layers[27,28]. These controllable properties of C_3N monolayer make it suitable for many applications, including Li-ion battery[29], metal-free catalyst[25], short channel transistors[24]. The ability to reversibly controlling the electronic properties in 2DM play a key role and dictate their potential future applications. In order to enhance the application of a material in electronic and optoelectronic devices, it can be very useful to regulate electronic properties. Bafekry *et al.* proposed that the electronic properties of 2D carbon nitride such as C_3N and C_2N monolayer can be tune via types of defects, adsorption/substitution of atoms applying an electric field or mechanical strain[30–35]. Types of vertical and in-plane strains, application of an electric field, doping, surface/edge functionalization, varying thickness of the 2DM, and heterostructuring, can tailor the electronic properties, which can be used for wide range of applications.[36–72].

In this work, the effect of B and N atoms doping on the electronic properties of graphene and C_3N monolayers, by using first-principle calculations is investigated. We found that B doped C_3N monolayer and B/N co-doped graphene bilayer are promising materials with semicounducting character exhibiting an direct band gap. The modulation of electronic properties via external means, including electric field (E-field), and different types of in-plane and out-of-plane strain (pressure) has been also investigated. We found that the electronic properties and even the nature of band gap of studied structures can be modulated by these approaches. Our results revealed that introduction of different atomic doping into C_3N and graphene lead to electronically tunable structures.

2 Method

All calculations in our work were performed by means of density functional theory (DFT), which was implemented in the OpenMX package[73]. The generalized gradient approximation (GGA), which is based on the Perdew-Burke-Ernzerhof (PBE)[74] was adopted for describing the exchange and correlation energies. The norm-conserving pseudopotentials[75] and pseudoatomic orbitals (PAOs)[76,77] were used to obtain the eigenvalues and eigenfunctions of the Kohn-Sham equations. The cutoff energy is set to be 400 eV. A $23 \times 23 \times 1$ Monkhorst-Pack k point grid[78] was used for sampling the first Brillouin zone. A periodic slab with a large vacuum layer of about 20 Å was applied along the z direction to break any unphysical interactions between adjacent layers. All the geometric optimization processes were fully relaxed until the atomic forces less than 1 meV/Å. The traditional GGA approximations are underestimated the long-range forces, thus the dispersion-corrected DFT-D2 method[79] was applied in layered systems. The optical calculations, such as real and imaginary parts of dielectric tensor and absorption coefficient were performed in the method constructed over the Perdew-Burke-Ernzerhof (PBE) functional. The optical properties were evaluated using a dense k-point grid of $10 \times 10 \times 1$-centered Monkhorst-Pack[78]. For more details about calculations of optical properties see supporting information (SI).

3 Doping of C_3N monolayer

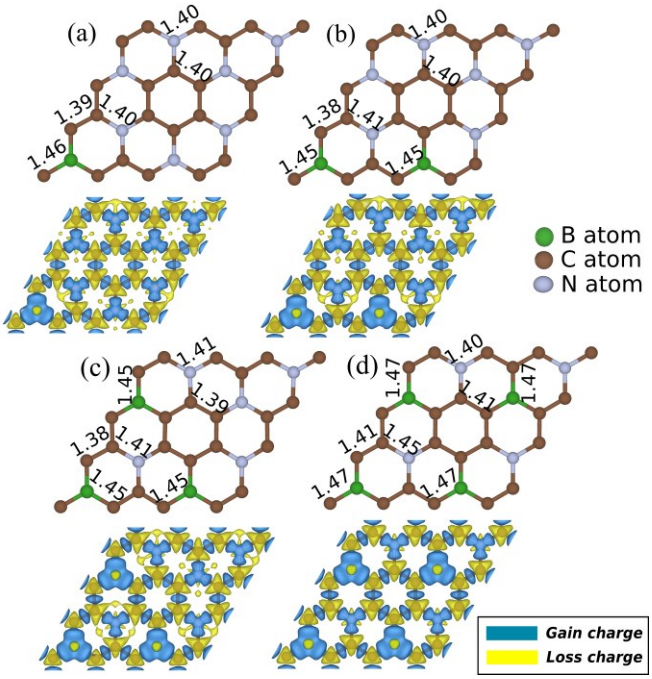

Fig. 1 Optimized structures of B doped C_3N monolayer with respect to concentration of (a) 3.1%, (b) 6.2%, (c) 9.3% and (d) 12.5%. The bond lengths of indicated in the same panel. Difference charge density is shown in the bottom of panel. The blue and yellow regions represent the charge accumulation and depletion, respectively.

We have systematically investigated the electronic properties of B and N atoms doping with different concentrations, on graphene and B atom on C_3N monolayers. Here, we have considered four concentration of B atom doped at the N-site of C_3N monolayer. Coverages of homogeneously arranged B doped atoms are from 3.1% to 12.5%. The atomic structure, electronic band structure with corresponding density of state (DOS) and partial DOS (PDOS) are shown in Figs. S1(a,b) in supplementary information (SI). The optimized lattice parameter and bond lengths of C-C and C-N bond are found to be 9.72, 1.42 and 1.42 Å, respectively. Our calculated band structure within PBE functional show that the C_3N monolayer is an indirect semiconductor with band gap of 0.4 eV. Notice that the conduction band minimum (CBM) and valence band maximum (VBM) are located at the Γ and K points, respectively. The VBM and CBM mainly originates from N-p_z and

Table 1 The structural and electronic parameters of B doped C_3 with different concentration is shown in Fig. 1(a). The corresponding structural and electronic parameters including the lattice constant (a); The bond length between atoms of C-C (d_{BC}), B-C (d_{BC}), N-C (d_{NC}) where distance are given in Å. Electronic states (ES) are specified as semiconductor (SC). The band gap is shown in parentheses and is given in eV.

Sys.	a	d_{CC}	d_{NC}	d_{BC}	E_C	ES
3.1%	9.72	1.39	1.40	1.46	-8.86	SC (0.42)
6.2%	9.72	1.38	1.41	1.45	-8.50	SC (0.37)
9.3%	9.72	1.38	1.41	1.45	-8.14	SC (0.65)
12.5%	9.96	1.41	1.45	1.47	-7.72	SC (1.30)

View Article Online
DOI: 10.1039/D0NJ03340E

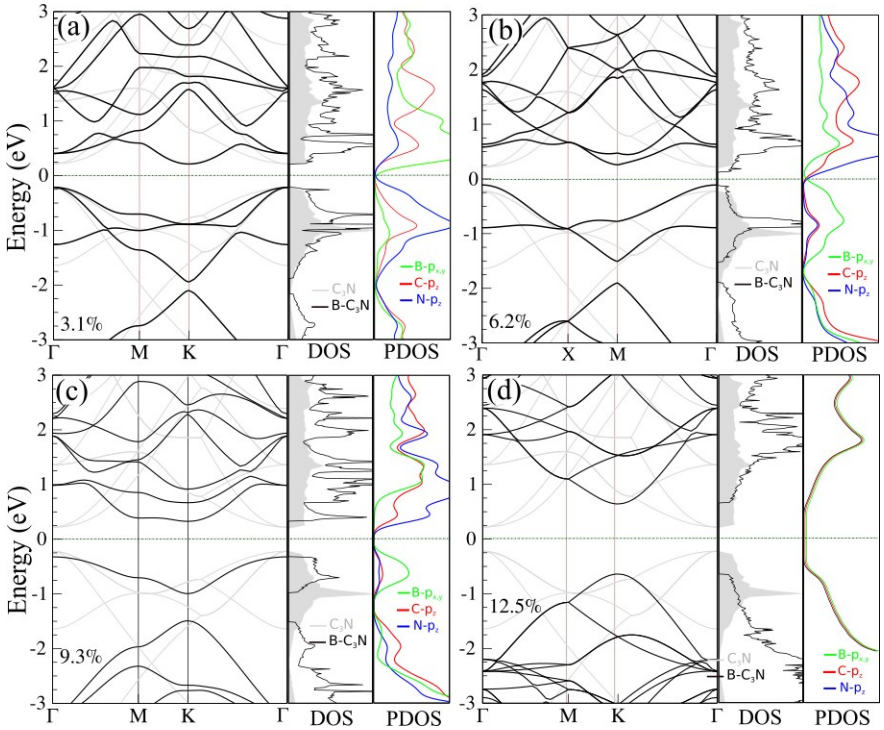

Fig. 2 Electronic band structure with corresponding DOS and PDOS of B doped C_3N monolayer with respect to concentration of (a) 3.1%, (b) 6.2%, (c) 9.3% and (d) 12.5%. The zero of energy is at Fermi-level.

C-p_z orbitals, respectively (see Fig. S1(a)). The optimized structures of B-C_3N with corresponding structural parameters for different concentrations are shown in Fig. 1. The C-B bond lengths are calculated 1.46 Å (at 3.1%) to 1.47 Å (at 12.5%) indicating that B is chemically substituted in C_3N. The bond lengths are in the range of 1.38-1.41 Å for C-C and 1.38-1.41 Å for C-N, while the C-C-C, C-B-C and C-N-C angles are 120°, displaying the characteristics of sp^2 hybridization. The cohesive energy were calculated using the following formula: $E_{coh} = \frac{E_{tot} - \sum n_B E_B}{N}$ where E_{tot}, E_B and n_B represents the total energy of B doped C_3N, atomic energy and the amount of B atoms, and N is the total number of atoms present in the C_3N monolayer, respectively. For the B-C_3N with 3.12% concentration, the cohesive energy is calculated to be E_{coh}=-8.95 eV/atom, which is lower than the cohesive energy of pristine C_3N (-9.32 eV/atom). In addition, our results shows that the cohesive energy of the B-C_3N were obtained to be -8.60 eV/atom (6.2%), -8.14 eV/atom (9.3%) and -7.65 eV/atom (12.5%).

The electronic band structure of C_3N monolayer with respect to B doped concentrations of 3.1%, 6.2%, 9.3% and 12.5% is shown in Fig. 2. For B-C_3N, from 3.1 to 6.2 %, we see a striking difference compared to pristine C_3N, although also a indirect band gap of 0.4 eV. One can observe that the band gap of C_3N monolayer is narrowed with the increasing B ratio, reflecting the delocalization of electronic states that is, the increase of interaction between C and N atoms in C_3N with the increase of B concentration. The finite of band gap is due to the reduced symmetry of the system after B doping. With the increasing the B concentration to 9.3%, the structure remains a indirect band gap of 0.65 eV, however with further increasing the B doping concentration up to 12.5%, the C_3N monolayer switched to direct nature of semiconductor with the band gap of 1.3 eV. It demonstrates that the conversion from indirect band gap to direct one can be achieved in C_3N monolayer by increasing the doping concentration. The band gap of C_3N monolayer is enlarged from 0.4 eV in pristine state to 1.3 eV with B doping concentration of 12.5 %. The semiconducting character of B doped C_3N is preserved in all case of different doping concentrations. The thermal stability of B-doped C_3N monolayer is verified by simulating *ab-initio* molecular dynamics (AIMD) calculations. As presented in Fig. S2 in SI, none of the monolayers undergo structural reconstructions even around 400 K indicating the thermal stability of each structure. In the Fig. S2, below each structural snapshots, the variation of total energy per atom in each structure is presented. Apparently, the change of the energy is almost 110 meV/atom. In addition, as the B-doping changes from 3.1% to 12.5%, the monolayer structure displays in-plane buckling with increasing temperature due to different B-C and C-N bond formations. It can be concluded that doped-graphene and B-doped C_3N structure exhibit thermal stability around the room temperature while increasing B-doping amount results in more in-plane buckling of the layer with increasing temperature.

4 Doping of graphene monolayer and bilayer

Here, we studied the effect especially pattern of B and N doped on graphene monolayer with concentration of 25%. The electronic band structure of B-N codoped graphene monolayer is shown in Fig. 3(a) and the optimized structure is shown in the inset. Our result show that the structural parameters including bond lengths

View Article Online
DOI: 10.1039/D0NJ03340E

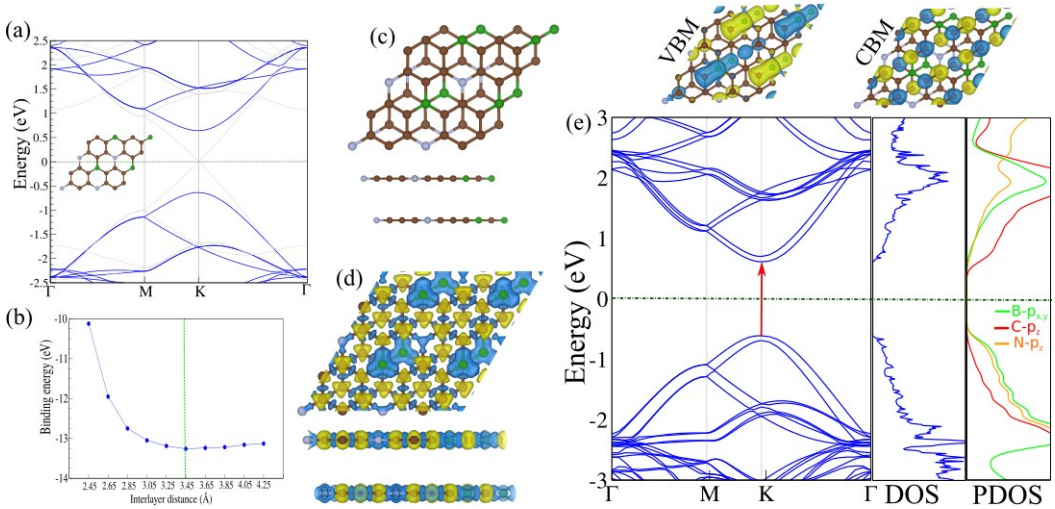

Fig. 3 (a) Electronic band structure of B-N doped graphene monolayer with concentration of 25% (b) Binding energy as functions of interlayer distance, (c) optimized structure, (d) difference charge density and (e) electronic band structure with corresponding DOS and PDOS for the B-N doped graphene bilayer. Charge densities of the VBM and CBM orbitals are shown in top of panel. Zero of energy is set to the Fermi level. The blue and yellow regions represent the charge accumulation and depletion, respectively.

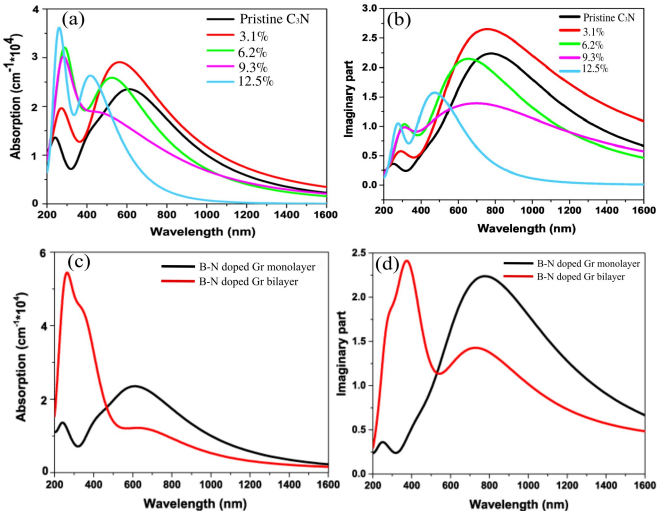

Fig. 4 Optical properties including: (a) optical absorption spectra, and (b) imaginary and real parts of the dielectric function ($\varepsilon(\omega_2)$) of B doped C_3N monolayer with respect to concentration of 3.1%, 6.2%, 9.3% and 12.5%. Optical properties as (c) optical absorption and (d) imaginary and real parts of B-N codoped graphene bilayer.

and bond angles is similar of B-C_3N with concentration 25%. The C-C, C-B and C-N bond lengths are 1.42, 1.48 and 1.46 Å, respectively, while the C-C-C, C-B-C and C-N-C angles are 120 °, displaying the characteristics of sp^2 hybridization. Our results show that B-N doping cause a weak structural distortion and the structure show a planar lattice. Interestingly, from the electronic structure, we found that energy bands are significantly affected by B and N doping. Notice the semi-metallic characteristic of pristine graphene transform to sectioning behavior, similar to the case of B-C_3N with 12.5 % dopant concentration. We can see that Dirac-point disappears completely and opened a direct band gap of 1.3 eV at the K point. This results in a electronic phase transition from semi-metal to semiconductor.

Before studying the electronic properties of the $BN-Gr@2L$, it is essential to approve its stability. This issue, the binding of the $BN-Gr@2L$ is estimated as function interlayer distance, as shown in Fig. 3(b). At equilibrium distance of 3.44 Å, the doped bilayer has a negative binding energy of 13.26 eV which the negative binding energy indicates the high structural stability of the constructed structure. Interestingly, the value of the binding energy keeps its negative sign for all interlayer distances without bonding contact between the bilayer, indicating the stability of the constructed bilayer at various interlayer distances from 2.25 Å to 4.5 Å The band structure of the $BN-Gr@2L$ is illustrated in Fig. 3(e). The doped bilayer is a semiconductor with direct band gap of 1.2 eV. This can be seen clearly from the locations of the valence band maximum (VBM) and conduction band minimum (CBM), where they are positioned at K point. The partial density of states revealed that the CBM and VBM of $BN-Gr@2L$ are dominated by p_z-orbitals (see Fig. 3(e)).

5 Optical properties

The optical properties of $B-C_3N@1L$ and $BN-Gr@2L$ were deliberated based on the obtained results of the imaginary part of the dielectric function ($\varepsilon(\omega)$) and absorption spectra. The frequency-dependent complex dielectric functions $\varepsilon(\omega) = \varepsilon_1(\omega) + i\varepsilon_2(\omega)$ are calculated. The imaginary part ε_2 can be derived from a summation over a satisfactorily large number of empty states, and the real part ε_1 is realized from the imaginary one by Kramer-Kronig relation, respectively. Additionally, the optical absorption coefficient $\alpha(\omega)$ was obtained from the dielectric components using the following expression,

$$\alpha(\omega) = \sqrt{2\omega}\sqrt{[\varepsilon_1^2(\omega)+\varepsilon_2^2(\omega)} - \sqrt{\varepsilon_1(\omega)} \quad (1)$$

where $\alpha(\omega)$, $\varepsilon_1(\omega)$, and $\varepsilon_2(\omega)$, stem for the absorption coefficient real part and imaginary part, respectively. Due to the potential applications in numerous optoelectronic devices, investi-

View Article Online
DOI: 10.1039/D0NJ03340E

gating the optical properties of multi-layers and monolayer sheets attract the attention of several scholars. The optical properties of pristine C_3N and doped C_3N monolayer with different B dopant concentrations have been studied based on the optical absorption spectra and imaginary part of the dielectric constant, as shown in Figs. 4(a,b). We can see two absorption peaks have been observed for C_3N and C_3N with different dopant concentrations. For C_3N monolayer, the strongest absorption peak is located in the visible range (600-700 nm), while a weak absorption peak is positioned in the UV region. Notice that with doing of C_3N structure, the absorption peak intensity in the visible range is decreased as compared to pristine C_3N. It is also observed that 3.1% B dopant concentration causes a red-shift as compared to the pristine monolayer. To get more insight into the effect of B doping on the optical properties of $BN-Gr@1L$ and $BN-Gr@2L$, the imaginary part and optical absorption spectra are studied, as shown in Fig. 4(c,d). We found that the $BN-Gr@1L$ has a stronger absorption spectrum in the UV region and it can be seen that the absorption spectrum of the doped bilayer is blue-shifted. This behavior has been expected because the doped bilayer structure has a wider band gap than that of the pristine. Notice that the

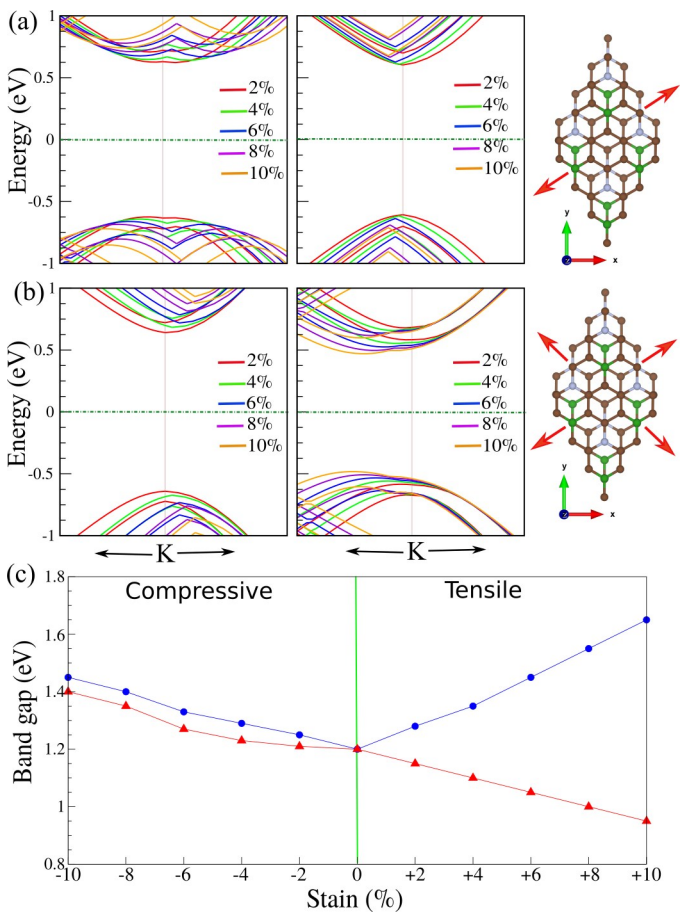

Fig. 5 Electronic band structure of $BN-Gr@2L$ as a function of the (a) uniaxial and (b) biaxial strain. The left and right are, respectively, tensile and compressive strain. Optimized structure and zoom of band structure under an electric field are shown in top of panel. Schematic model of the $BN-Gr@2L$ structure with applied strain indicated in the right panel. (c) Variations of band gap with respect to both uniaxial and biaxial strains.

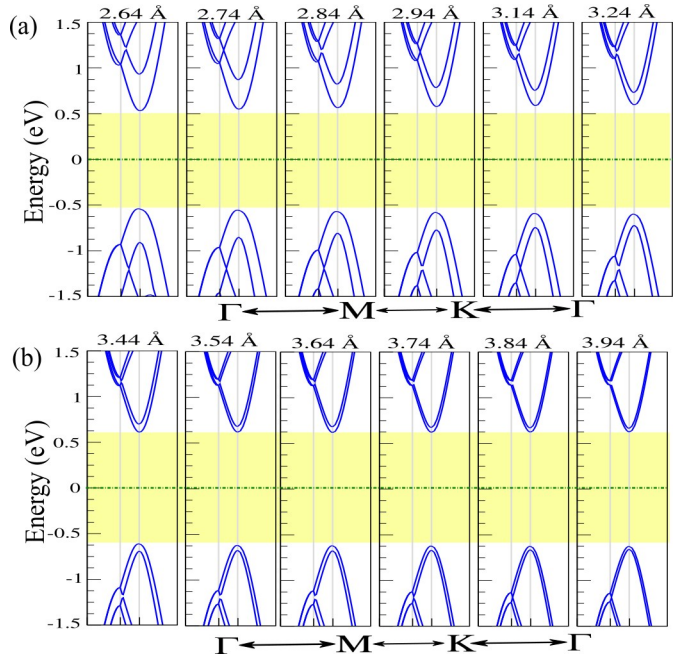

Fig. 6 Electronic band structure of the $BN-Gr@2L$ under (a) negative and (b) positive vertical strain. Zero of energy is set to the Fermi level.

$BN-Gr@2L$ has the most efficient absorption capability as compared to its pristine structure. It has a broad absorption spectrum in a wide visible range start from 400 nm to 1000 nm with strong absorption intensity.

6 Effect of strain on doped graphene bilayer

In the following, we investigated the effect of uniaxial and biaxial strain on the electronic structure of $BN-Gr@2L$. The top and side views of AA (left) and AB (right) stacking arrangements of B/N-doped graphene bilayer is shown in Fig. S3 in (SI). The strain is defined as $\varepsilon = (a \pm a_0)/a_0 \times 100$, where a and a_0 are the strained and non-strained lattice constants, respectively, and the positive (negative) sign denotes tensile (compressive) strain. Uniaxial strain is applied along zigzag direction, while biaxial strain is applied along a-b axis. The electronic band structure under uniaxial and biaxial strain are shown in Figs. 5(a) and 5(b), respectively. The schematic model of the $BN-Gr@2L$ structure with applied strain is in the right panel in Fig. 5. Notice that $BN-Gr@2L$ is initially a semiconductor and has a direct band gap of 1.2 eV. With increasing uniaxial strain from +2 to +8% the direct band gap increases to 1.3 eV (at +2%), 1.35 eV (at +4%), 1.45 eV (at +6%), 1.55 eV (at +8%) and 1.65 eV (at +10%) and its semiconducting character is preserved. This situation is different for the compression strain, so upon a biaxial strain -2% $BN-Gr@2L$ is a semiconductor with a direct band gap of 1.25 eV and with increasing magnitude of compressive strain from -4 to -10%, the band gaps are obtained 1.3 eV(-4%) to 1.45 eV (-10%) and the VBM and CBM will move slightly from the **K**-point in the BZ (see Fig. 6(a)). The electronic band structure of $BN-Gr@2L$ under biaxial tensile and compressive strains is shown in Fig. 6. Our results show that $BN-Gr@2L$, the band gap under biaxial tensile (compressive) strain, decreases (increase), while the VBM

View Article Online
DOI: 10.1039/D0NJ03340E

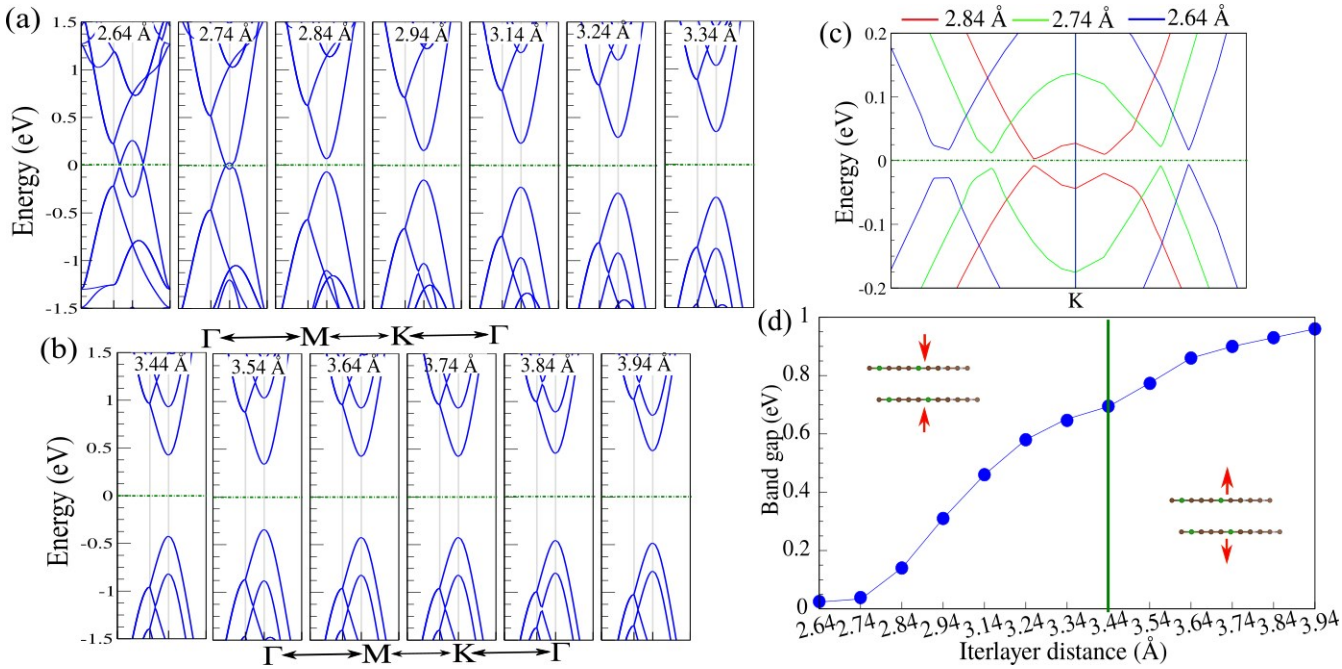

Fig. 7 Electronic band structure of the $BN-Gr@2L$ (at AA stacking) under (a) negative and (b) positive vertical strain. (c) Zoom of band structure for the different interlayer distances. Zero of energy is set to the Fermi level. (d) Variation of the band gap as a function interlayer distance.

and CBM position small shift from the **K**-point. With increasing of biaxial strain as tensile, the band gap decreases to 1.15 eV (at +2%), 1.1 eV (at +4%), 1.05 eV (at +6%), 1 eV (at +8%) and 0.9 eV (at +10%) and the VBM and CBM will small shift from the **K**-point. We found that the direct band gap increases with increasing compressive biaxial strain to 1.21 eV (at -2%) and 1.25 eV (at -4%). The semiconducting character is preserved for the magnitude of strains larger than -2%, while for the large strain ($> -6\%$) a direct band gaps are determined 1.30 (at -6%), 1.35 (at -8%). 1.40 (at -10%). The variations of band gap with respect to both uniaxial and biaxial strains are shown in Fig. 5(c). Notice that under large biaxial strain, remains semiconductor for the both tensile and compressive. These results reveal strain engineering dependent band gaps and electronic structure in the $BN-Gr@2L$ could be of use in high-performance electronic and optoelectronic devices.

The impacts of vertical strain on the electronic band structure of $BN-Gr@2L$ are studied by decreasing or increasing the vertical distance between the two BN doped graphene layers. This can be defined as $\varepsilon = (h \pm h_0)/h_0$, where h and h_0 are the equilibrium and fixed interlayer distances, respectively. The electronic band structure of the $BN-Gr@2L$ under negative and positive vertical strain are shown in Fig. 7(a,b), respectively. One can find that he interlayer coupling can not tune the band gap of $BN-Gr@2L$ part and the semiconducting characteristic is preserved with decrease and increases of the interlayer distance. When the interlayer coupling is strengthened, i.e the interlayer distance is decreased, one can observe that the band gap of $BN-Gr@2L$ is decreased from 1.17 eV (at 3.34 Å) to 1.02 eV (at 2.64 Å). We can see that the energy bands of the VBM and CBM are splitted, respectively, in around of -0.5 and +0.5 eV below the Fermi-level. In contrast, when the interlayer coupling is weakened, i.e the interlayer distance is increased, the band gap of $BN-Gr@2L$ is small increase from 1.2 eV (at 3.44 Å) to 1.22 eV (at 3.84 Å). More interestingly, the weakened interlayer coupling dose not shifts the VBM and CBM positions, resulting in the direct band gap of $BN-Gr@2L$ is preserved (see Fig. 7(b)). Therefore, we can conclude that the interlayer coupling cant strongly tune the band gap of $BN-Gr@2L$ and the band gaps can be remain about 1.2 eV.

The electronic band structure of the B-N doped graphene bilayer (at AA stacking) under negative and positive vertical strain are shown in Figs. 7(a,b), respectively. As shown in Fig. 7(a), the negative vertical strain has a significant influence on the electronic band structure of the doped bilayer. At a strain of 0.23 (2.75 Å) and 0.30 (2.5 Å), the strained doped bilayer structures have a Dirac-like cone near K-point with band gap values of 4 meV and 50 meV, respectively. At a higher negative strain of 0.37 (2.25 Å), the doped bilayer has a metallic character with a zero band gap. In contrast, the positive strain has a mild influence on the electronic properties of the doped bilayer structure, as shown in Fig. 7(b). It can be seen that band gap value increases as the positive strain increases. The inset of band structure for the different interlayer distances is shown in Fig. 7(c). The influence of the negative and positive strains is shown in Fig. 7(d), where suitable band gap values ranging from 0-1.16 eV can be achieved at various interlayer distances.

7 Conclusion

In conclusion, we have investigated the structural, electronic and optical properties of the B doped C_3N monolayer (B-C_3N) and B-N doped graphene bilayer ($BN-Gr@2L$) sing first principles calculations. Our results demonstrate that both B doping with different concentrations leads to an band gap increasing in C_3N mono-

View Article Online
DOI: 10.1039/D0NJ03340E

layer. The transition from indirect semiconductor to direct one is observed in C_3N monolayer with the 12.5 % B dopant concentration. In addition a semi-metal to semiconductor transformation is achieved in graphene monolayer with the B and N codoping in the hexagonal pattern. Furthermore, the B-C_3N monolayer and $BN-Gr@2L$ tends to an increase in the optical absorption intensity with a wide visible range start from 400 nm to 1000 nm. Our theoretical results shows that the electronic properties of single layers of C_3N and graphene, strongly depend on the dopant concentration in the hexagonal doping pattern. Moreover, our results show that both in-plane and out-of-plane strains can tune both the electronic properties and band edges positions of the $BN-Gr@2L$ and interestingly we found a electronic transition from semiconductor to semi-metal is occurred. The controllable electronic and optical properties of the $BN-Gr@2L$ by strain engineering may facilitate their practical performance for the future applications.

Conflicts of interest

The authors declare that there are no conflicts of interest regarding the publication of this paper.

Acknowledgments

This work has supported by the National Research Foundation of Korea(NRF) grant funded by the Korea government(MSIT)(NRF-2017R1A2B2011989).

Data Availability Statement

All data generated or analyzed during this study are included in this published article (and its Supplementary Information Files).

References

1 K. S. Novoselov, A. K. Geim, S. V. Morozov, D. Jiang, Y. Zhang, S. V. Dubonos, I. V. Grigorieva and A. A. Firsov, *Science*, 2004, **306**, 666–669.
2 Z. Cai, B. Liu, X. Zou and H.-M. Cheng, *Chemical reviews*, 2018, **118**, 6091–6133.
3 G. Fiori, F. Bonaccorso, G. Iannaccone, T. Palacios, D. Neumaier, A. Seabaugh, S. K. Banerjee and L. Colombo, *Nature nanotechnology*, 2014, **9**, 768.
4 F. Koppens, T. Mueller, P. Avouris, A. Ferrari, M. Vitiello and M. Polini, *Nature nanotechnology*, 2014, **9**, 780.
5 B. Mendoza-Sánchez and Y. Gogotsi, *Advanced Materials*, 2016, **28**, 6104–6135.
6 Y. Kubota, K. Watanabe, O. Tsuda and T. Taniguchi, *Science*, 2007, **317**, 932–934.
7 G. Cassabois, P. Valvin and B. Gil, *Nature Photonics*, 2016, **10**, 262.
8 A. Carvalho, M. Wang, X. Zhu, A. S. Rodin, H. Su and A. H. C. Neto, *Nature Reviews Materials*, 2016, **1**, 1–16.
9 Z. Ma, B. Wang, L. Ou, Y. Zhang, X. Zhang and Z. Zhou, *Nanotechnology*, 2016, **27**, 415203.
10 H.-P. Komsa, J. Kotakoski, S. Kurasch, O. Lehtinen, U. Kaiser and A. V. Krasheninnikov, *Physical review letters*, 2012, **109**, 035503.
11 D. Jariwala, V. K. Sangwan, L. J. Lauhon, T. J. Marks and M. C. Hersam, *ACS nano*, 2014, **8**, 1102–1120.
12 Q. H. Wang, K. Kalantar-Zadeh, A. Kis, J. N. Coleman and M. S. Strano, *Nature nanotechnology*, 2012, **7**, 699.
13 H. Wang, H. Yuan, S. S. Hong, Y. Li and Y. Cui, *Chemical Society Reviews*, 2015, **44**, 2664–2680.
14 Y. Zhang, J. Liu, G. Wu and W. Chen, *Nanoscale*, 2012, **4**, 5300–5303.
15 K. Srinivasu, B. Modak and S. K. Ghosh, *The Journal of Physical Chemistry C*, 2014, **118**, 26479–26484.
16 S. Y. Zhou, G.-H. Gweon, A. Fedorov, d. First, PN, W. De Heer, D.-H. Lee, F. Guinea, A. C. Neto and A. Lanzara, *Nature materials*, 2007, **6**, 770–775.
17 K. F. Mak, C. Lee, J. Hone, J. Shan and T. F. Heinz, *Physical review letters*, 2010, **105**, 136805.
18 B. Radisavljevic, A. Radenovic, J. Brivio, V. Giacometti and A. Kis, *Nature nanotechnology*, 2011, **6**, 147.
19 J. Mahmood, E. K. Lee, M. Jung, D. Shin, I.-Y. Jeon, S.-M. Jung, H.-J. Choi, J.-M. Seo, S.-Y. Bae, S.-D. Sohn *et al.*, *Nature communications*, 2015, **6**, 6486.
20 B. Mortazavi, *Carbon*, 2017, **118**, 25–34.
21 X. Wang, K. Maeda, A. Thomas, K. Takanabe, G. Xin, J. M. Carlsson, K. Domen and M. Antonietti, *Nature materials*, 2009, **8**, 76–80.
22 J. Mahmood, E. K. Lee, M. Jung, D. Shin, H.-J. Choi, J.-M. Seo, S.-M. Jung, D. Kim, F. Li, M. S. Lah *et al.*, *Proceedings of the National Academy of Sciences*, 2016, **113**, 7414–7419.
23 S. Yang, W. Li, C. Ye, G. Wang, H. Tian, C. Zhu, P. He, G. Ding, X. Xie, Y. Liu *et al.*, *Advanced Materials*, 2017, **29**, 1605625.
24 L.-B. Shi, Y.-Y. Zhang, X.-M. Xiu and H.-K. Dong, *Carbon*, 2018, **134**, 103–111.
25 B. He, J. Shen, D. Ma, Z. Lu and Z. Yang, *The Journal of Physical Chemistry C*, 2018, **122**, 20312–20322.
26 D. Wang, Y. Bao, T. Wu, S. Gan, D. Han and L. Niu, *Carbon*, 2018, **134**, 22–28.
27 C. Zhang, Y. Jiao, T. He, S. Bottle, T. Frauenheim and A. Du, *The journal of physical chemistry letters*, 2018, **9**, 858–862.
28 J. Zhao, H. Zeng and X. Zhou, *Carbon*, 2019, **145**, 1–9.
29 J. Xu, J. Mahmood, Y. Dou, S. Dou, F. Li, L. Dai and J.-B. Baek, *Advanced Materials*, 2017, **29**, 1702007.
30 A. Bafekry, S. Farjami Shayesteh and F. M. Peeters, *J. Phys. Chem. C*, 2019, **123**, 12485–12499.
31 A. Bafekry and M. Neek-Amal, *Phys. Rev. B*, 2020, **101**, 085417.
32 A. Bafekry, S. F. Shayesteh and F. M. Peeters, *Phys. Chem. Chem. Phys.*, 2019, **21**, 21070–21083.
33 A. Bafekry, M. Ghergherehchi, S. F. Shayesteh and F. Peeters, *Chem. Phys.*, 2019, **526**, 110442.
34 A. Bafekry, C. Stampfl and S. Farjami Shayesteh, *ChemPhysChem*, 2020, **21**, 164–174.
35 A. Bafekry, C. Stampfl, M. Ghergherehchi and S. F. Shayesteh, *Carbon*, 2020, **157**, 371–384.
36 W. Reckien, F. Janetzko, M. F. Peintinger and T. Bredow, *Journal of Computational Chemistry*, 2012, **33**, 2023–2031.

View Article Online
DOI: 10.1039/D0NJ03340E

37 A. Bafekry, S. Farjami Shayesteh, M. Ghergherehchi and F. M. Peeters, *J. Appl. Phys.*, 2019, **126**, 144304.
38 Ilawe Niranjan V., Zimmerman Jonathan A. and Wong Bryan M., *Journal of Chemical Theory and Computation*, 2015, **11**, 5426–5435.
39 A. Bafekry, C. Stampfl, B. Akgenc and M. Ghergherehchi, *Phys. Chem. Chem. Phys.*, 2020, **22**, 2249–2261.
40 M. Sun, W. Tang, Q. Ren, S. ke Wang, J. Yu and Y. Du, *Applied Surface Science*, 2015, **356**, 110 – 114.
41 A. Bafekry, S. F. Shayesteh and F. M. Peeters, *J. Appl. Phys.*, 2019, **126**, 215104.
42 M. Sun, Y. Hao, Q. Ren, Y. Zhao, Y. Du and W. Tang, *Solid State Communications*, 2016, **242**, 36 – 40.
43 A. Bafekry, *Physica E*, 2020, **118**, 113850.
44 S. W. J. Y. W. T. M. Sun, Q. Ren, *Journal of Physics D: Applied Physics*, 2016, **49**, 445305.
45 A. Bafekry, C. Stampfl, B. Akgenc, B. Mortazavi, M. Ghergherehchi and C. V. Nguyen, *Phys. Chem. Chem. Phys.*, 2020, **22**, 6418–6433.
46 S. Wang, H. Tian, Y. Luo, J. Yu, C. Ren, C. Sun, Y. Xu and M. Sun, *Applied Surface Science*, 2019, **481**, 1549 – 1553.
47 A. Bafekry, B. Akgenc, S. F. Shayesteh and B. Mortazavi, *Appl. Surf. Sci.*, 2020, **505**, 144450.
48 Shu Huabing, Zhao Minglin and Sun Minglei, *ACS Applied Nano Materials*, 2019, **2**, 6482–6491.
49 A. Bafekry and M. Neek-Amal, *Phys. Rev. B*, 2020, **101**, 085417.
50 M. Sun, J.-P. Chou, J. Yu and W. Tang, *J. Mater. Chem. C*, 2017, **5**, 10383–10390.
51 A. Bafekry, C. Stampfl and F. M. Peeters, *Sci. Rep.*, 2020, **10**, 1–15.
52 M. Sun, J.-P. Chou, Q. Ren, Y. Zhao, J. Yu and W. Tang, *Applied Physics Letters*, 2017, **110**, 173105.
53 B. Mortazavi, A. Bafekry, M. Shahrokhi, T. Rabczuk and X. Zhuang, *Mater. Today Energy*, 2020, **16**, 100392.
54 M. Sun, J.-P. Chou, Y. Zhao, J. Yu and W. Tang, *Phys. Chem. Chem. Phys.*, 2017, **19**, 28127–28132.
55 A. Bafekry, M. Ghergherehchi and S. F. Shayesteh, *Phys. Chem. Chem. Phys.*, 2019, **21**, 10552–10566.
56 S. Lu, C. Li, H. Li, Y. Zhao, Y. Gong, L. Niu, X. Liu and T. Wang, *Applied Surface Science*, 2017, **392**, 966 – 974.
57 A. Bafekry, B. Mortazavi and S. F. Shayesteh, *J. Magn. Mag. Mater.*, 2019, **491**, 165565.
58 H. Li, Y. Wu, C. Li, Y. Gong, L. Niu, X. Liu, Q. Jiang, C. Sun and S. Xu, *Applied Catalysis B: Environmental*, 2019, **251**, 305 – 312.
59 A. Bafekry, C. Stampfl and F. M. Peeters, *Phys. Status Solidi B Basic Res.*, 2020, **257**, 2000182.
60 K. Zhour, F. El Haj Hassan, H. Fahs and M. Vaezzadeh, *Materials Today Communications*, 2019, **21**, 100676.
61 A. Bafekry, B. Akgenc, M. Ghergherehchi and F. Peeters, *J. Phys.: Condens. Matt.*, 2020, **32**, 355504.
62 Q. Li, Q. Li, H. Wang and H. Pan, *Physica B: Condensed Matter*, 2020, **577**, 411807.
63 A. Baafekry, M. Yagmurcukardes, B. Akgenc, M. Ghergherehchi and C. Nguyen, *J. Phys. D: Appl. Phys.*, 2020, **53**, year.
64 H. Wang, Q. Li, H. Pan, Y. Gao and M. Sun, *Journal of Applied Physics*, 2019, **126**, 234302.
65 A. Bafekry, C. Stampfl and M. Ghergherehchi, *Nanotechnology*, 2020, **31**, 295202.
66 X. Wang, Q. Li, H. Wang, Y. Gao, J. Hou and J. Shao, *Physica B: Condensed Matter*, 2018, **537**, 314 – 319.
67 A. Bafekry, M. Neek-Amal and F. Peeters, *Phys. Rev. B*, 2020, **101**, 165407.
68 Y. Wu, C. Li, W. Liu, H. Li, Y. Gong, L. Niu, X. Liu, C. Sun and S. Xu, *Nanoscale*, 2019, **11**, 5064–5071.
69 M. M. Obeid, C. Stampfl, A. Bafekry, Z. Guan, H. R. Jappor, C. V. Nguyen, M. Naseri, D. M. Hoat, N. N. Hieu, A. E. Krauklis, T. V. Vu and D. Gogova, *Phys. Chem. Chem. Phys.*, 2020, **22**, 15354–15364.
70 A. Bafekry, M. M. Obeid, C. V. Nguyen, M. Ghergherehchi and M. Bagheri Tagani, *J. Mater. Chem. A*, 2020, **8**, 13248–13260.
71 A. Bafekry, M. Yagmurcukardes, M. Shahrokhi and M. Ghergherehchi, *Carbon*, 2020, **168**, 220 – 229.
72 A. Bafekry, C. V. Nguyen, A. Goudarzi, M. Ghergherehchi and M. Shafieirad, *RSC Adv.*, 2020, **10**, 27743–27751.
73 T. Ozaki, K. Nishio and H. Kino, *Phys. Rev. B*, 2010, **81**, 035116.
74 J. P. Perdew, K. Burke and M. Ernzerhof, *Physical Review Letters*, 1996, **77**, 3865.
75 N. Troullier and J. L. Martins, *Physical Review B*, 1991, **43**, 1993.
76 T. Ozaki, *Physical Review B*, 2003, **67**, 155108.
77 T. Ozaki and H. Kino, *Physical Review B*, 2004, **69**, 195113.
78 H. J. Monkhorst and J. D. Pack, *Physical Review B*, 1976, **13**, 5188.
79 S. Grimme, *Journal of Computational Chemistry*, 2006, **27**, 1787–1799.